SUBCRITICAL SPATIAL TRANSITION OF SWEPT HIEMENZ FLOW

Dominik Obrist
Institute of Fluid Dynamics
ETH Zurich
8092 Zurich, Switzerland
obristd@ethz.ch

Rolf Henniger
Institute of Fluid Dynamics
ETH Zurich
8092 Zurich, Switzerland
hennigerr@ethz.ch

Leonhard Kleiser
Institute of Fluid Dynamics
ETH Zurich
8092 Zurich, Switzerland
kleiser@ethz.ch

ABSTRACT

It is known from experimental investigations that the leading-edge boundary layer exhibits transition to turbulence at subcritical Reynolds numbers, i.e. at Reynolds numbers which lie below the critical Reynolds number predicted by linear stability theory. In the present work, we investigate this subcritical transition process by direct numerical simulations of a swept Hiemenz flow in a spatial setting. The laminar base flow is perturbed upstream by a pair of stationary counter-rotating vortices. This perturbation generates high- and low-speed streaks by a non-modal growth mechanism. Further downstream, these streaky structures exhibit a strong instability to secondary perturbations which leads to a breakdown to turbulence.

The observed transition mechanism has strong similarities to by-pass transition mechanisms found for two-dimensional boundary layers. It can be shown that the transition strongly depends on the amplitude of the primary perturbation as well as on the frequency of the secondary perturbation.

INTRODUCTION

Swept Hiemenz flow serves as a model for the leading-edge boundary layer in the vicinity of the stagnation line of a swept wing. Experiments by Poll (1979) indicated that the swept leading-edge boundary layer can experience transition to turbulence at Reynolds numbers as low as 250 (where the Reynolds number $\mathrm{Re} = W_\infty^*/\sqrt{S^*\nu^*}$ is defined on the basis of the free-stream sweep velocity W_∞^*, the free-stream shear rate S^* and the kinematic viscosity ν^*). Linear theory, however, predicts stability for swept Hiemenz flow up to $\mathrm{Re} = 581$ (Hall *et al.*, 1984). A weakly nonlinear subcritical instability mechanism was proposed by Hall & Malik (1986) which helped to reduce the theoretical critical Reynolds number somewhat. Further theoretical advances were achieved, for instance, by Lin & Malik (1996) and later also by Theofilis *et al.* (2003) who investigated modes of higher polynomial order in the chordwise direction. It was shown by Obrist & Schmid (2003*b*) that these modes can exhibit strong transient growth. Optimal disturbances for the spatial stability problem were found by Guégan *et al.* (2008). Despite these and several other studies, no theoretical work has been able so far to explain the large discrepancy between the theoretical results and the experimental observations by Poll (1979).

Next to experimental and theoretical investigations, some results from direct numerical simulations (DNS) and large-eddy simulations (LES) of swept Hiemenz flow exist. Spalart (1988) presented the first DNS in a temporal setting, i.e. with periodicity in the spanwise direction. Obrist & Schmid (2003*b*) used a DNS to study the receptivity for spanwise vortical disturbances in the free-stream. For spatial configurations, i.e. with an non-periodic spanwise direction, the DNS by Joslin (1995) and the LES by Dimas *et al.* (2003) are available. These simulations used 'vibrating ribbons' to create localized disturbances which propagate and grow in the downstream (span- and chordwise) direction. Both simulations were strongly limited by the available computational power such that none of these simulations was able to illustrate the full transition process.

In the present work, we perform a series of DNS in a spatial configuration at a subcritical Reynolds number of $\mathrm{Re} = 300$. We demonstrate how a pair of counter-rotating streamwise vortices creates streaks of streamwise velocity in the boundary layer which exhibit a secondary instability leading to transition to turbulence.

NUMERICAL METHODS

The DNS are carried out with a high-fidelity solver for the Navier–Stokes equations (Henniger *et al.*, 2010*b*) which uses high-order finite differences in all three directions and is optimized for massively parallel computing. The chordwise coordinate x is perpendicular to the attachment line and par-

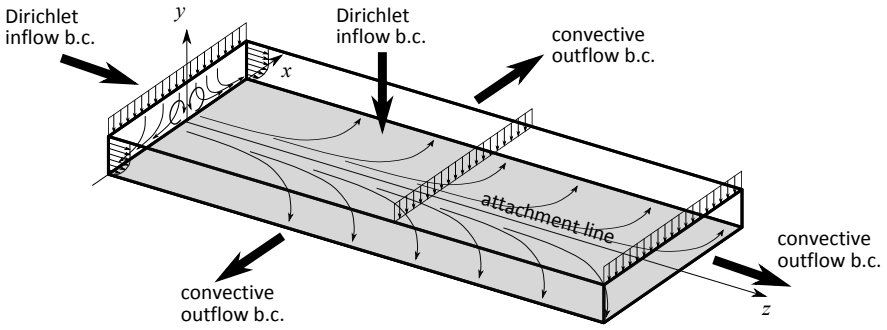

Figure 1. Computational domain with in- and outflow boundary conditions and the counter-rotating pair of streamwise vortices at the inflow.

allel to the wall, y is the wall-normal coordinate and z points in the spanwise direction along the attachment line (figure 1). The computational domain of size $150 \times 22.5 \times 600$ covers a finite section of the attachment line and its vicinity (using $L^* = \sqrt{\nu^*/S^*}$ as reference length). In the wall-normal direction, it reaches well beyond the boundary layer ($\delta^* \approx 3L^*$) into the free-stream. This flow field is discretized on a grid with $513 \times 49 \times 1537$ points. Grid stretching in the wall-normal direction ensures a well-resolved boundary layer.

The base flow configuration is enforced by Dirichlet boundary conditions at the spanwise and at the wall-normal inflow boundary. The outflow at the spanwise end and at both chordwise boundaries is realized by convective outflow boundary conditions which have been shown (e.g. Henniger *et al.*, 2010*a*) to yield a clean outflow of perturbations with very little or no influence on the upstream flow field. The present numerical set-up has been validated for swept Hiemenz flow by simulating the spatial decay of linear eigensolutions of Görtler–Hämmerlin type (Theofilis, 1995).

Inflow and initial conditions

The inflow is perturbed with a pair of stationary counter-rotating streamwise vortices of the form $[u'(x,y), v'(x,y), 0]^T$ with the amplitude A_1. This perturbation is motivated by Guégan *et al.* (2008) who showed that such vortices are nearly optimal spatial disturbances for swept Hiemenz flow. Similar to the process in two-dimensional boundary layers, such vortices lead to a strong linear transient growth of the disturbance energy by creating low/high-speed streaks through the lift-up effect (Landahl, 1980).

In order to obtain an unsteady breakdown of the streaks we introduce a weak secondary perturbation with an amplitude A_2 by modulating the amplitude of the streamwise vortices at a well-defined frequency f_0. The complete inflow perturbation then reads

$$(A_1 + A_2 \sin 2\pi f_0 t) \cdot [u'(x,y), v'(x,y), 0]^T \qquad (1)$$

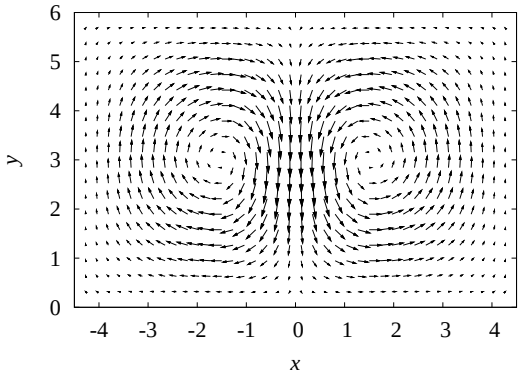

Figure 2. Flow field of the perturbation which is superimposed at the inflow boundary onto the base flow solution.

where

$$u'(x,y) = -\frac{1}{2}\sin\frac{\pi(y-y_c)}{b}\left[1+cos\frac{\pi(x-x_c)}{b}\right] + \frac{1}{2}\sin\frac{\pi(y-y_c)}{b}\left[1+cos\frac{\pi(x+x_c)}{b}\right] \qquad (2a)$$

$$v'(x,y) = \frac{1}{2}\sin\frac{\pi(x-x_c)}{b}\left[1+cos\frac{\pi(y-y_c)}{b}\right] - \frac{1}{2}\sin\frac{\pi(x+x_c)}{b}\left[1+cos\frac{\pi(y-y_c)}{b}\right] \qquad (2b)$$

for $|x-x_c| < b$ and $|y-y_c| < b$; otherwise $u' = v' = 0$.

In the present simulations, we choose the center of the vortices at $(\pm x_c, y_c) = (\pm 1.5, 3)$ with a half-width of $b = 3$. In this configuration the centers of the two counter-rotating vortices are at the edge of the spanwise boundary layer. The vortices overlap in the middle such that they create a significant flow toward the wall at the attachment line (figure 2).

The simulations are started from an unperturbed initial flow field. The inflow boundary condition (1) creates two counter-rotating streamwise vortices which propagate and evolve into the computational domain. The simulation is continued until a statistically steady configuration is reached.

Energy metric

The statistically steady flow field is analyzed by performing a modal decomposition into energy densities. To this end, we subtract the base flow solution from the flow field and perform a discrete Fourier transform in time as well as an expansion into Hermite polynomials $\mathrm{He}_n(x)$ in the chordwise direction. This leads to modal energy densities e_{kn} (Obrist & Schmid, 2003*b*),

$$e_{kn}(z) = \int_0^\infty |\hat{u}_{kn}|^2 + |\hat{v}_{k(n-1)}|^2 + |\hat{w}_{k(n-1)}|^2 \mathrm{d}y, \qquad (3)$$

where the index k indicates the frequency kf_0 and n the order of the Hermite polynomial, i.e.

$$\hat{u}_{kn}(y,z) = f_0 \int_{t_1}^{t_1+1/f_0} \mathrm{e}^{-\mathrm{i}2\pi f_0 k t} \mathrm{d}t \int_{-L_x}^{L_x} u(x,y,z,t)\mathrm{He}_n(x) \cdot \mathrm{e}^{-(x/\gamma)^2/2} \mathrm{d}x. \qquad (4)$$

The parameter γ determines the width of the Gaussian kernel in the Hermite expansion. Here, we choose $\gamma = 10$ which includes most of the computational domain into the energy densities but ensures that artifacts at the chordwise boundaries do not influence the results.

Note that the energy density (3) is defined such that the polynomial order n of the chordwise velocity u is combined with the polynomial order $n-1$ of the wall normal and spanwise velocities, v and w. This choice is motivated by the structure of the linear modes of the swept Hiemenz flow (Obrist & Schmid, 2003*a*). The Görtler–Hämmerlin modes, for instance, are linear in x for the chordwise velocity u and constant in x for v and w. The energy of such perturbations is contained in the energy densities e_{k1}.

The modes of odd polynomial order in u preserve the symmetry of the base flow configuration. Therefore, we call these modes symmetric modes. Their energy is represented by the energy densities $e_{k1}, e_{k3}, e_{k5}, \ldots$. The anti-symmetric modes break the symmetry of the swept Hiemenz flow with respect to the attachment line. Their energy is contained in $e_{k0}, e_{k2}, e_{k4}, \ldots$.

RESULTS

We present results of several DNS at $\mathrm{Re} = 300$ with different amplitudes and frequencies (table 1). According to linear stability theory, the flow is stable at this Reynolds number such that only nonlinear instabilities can lead to transition to turbulence. Therefore, the primary disturbance amplitude is chosen such that the velocities of the streamwise vortices at the inflow reach about 10% of the free-stream sweep velocity. Despite this relatively large amplitude of the primary disturbance, we do not observe the onset of a transition for this perturbation alone. Instead, the pair of streamwise vortices separates at the attachment line and each vortex follows roughly the divergent inviscid streamlines of the base flow.

In order to obtain transition to turbulence, we need to add a secondary perturbation at the inflow by modulating the amplitude of the primary vortices (1). These secondary perturbations are weak, i.e. on the order of 0.1 to 1% of the free-stream sweep velocity.

Table 1. Simulation parameters.

	A_1	A_2	f_0
slow I	0.05	0.005	$1/60$
slow II	0.07	0.007	$1/60$
slow III	0.1	0.01	$1/60$
slow IV	0.1	0.001	$1/60$
medium	0.1	0.001	$1/30$
fast	0.1	0.001	$1/10$

Figure 3 shows the vortical structures for a simulation with a secondary perturbation. We observe a successive breakdown of the streamwise vortices toward a turbulent boundary layer at the spanwise end of the computational domain.

To investigate the dependence of the transition process on the frequency f_0, we show in figure 4 snapshots of the streamwise velocity w in a plane parallel to the wall at $y = 1$ (within the boundary layer). Each snapshot corresponds to a different secondary perturbation frequency f_0. In all three simulations, the streamwise vortices rapidly create streaks along the attachment line by the lift-up effect. This yields a high-speed streak along the attachment line and two low-speed streaks to the left and right. The divergent character of the swept Hiemenz flow pulls these streaky structures apart as the disturbance evolve in the downstream direction.

With the fastest secondary perturbation (figure 4c), the streaks remain laminar and are eventually washed out of the domain. This suggests that the frequency of the secondary perturbation is too high for the given primary perturbation.

For the two slower secondary perturbations (figure 4 a & b), we can observe varicose secondary instabilities after $z \approx 100$ which grow rapidly and eventually lead to a breakdown to a turbulent flow beyond $z \approx 500$. The turbulent region grows in the chordwise direction roughly along the inviscid streamlines.

The mechanism of the transition process is more evident in figure 5 which shows modal energies (3) for the *medium* simulation. The rapid growth of the stationary modes e_{01} and e_{03} for $0 < z < 30$ is due to the strong transient linear growth mechanism which generates the streaks (lift-up effect). After the saturation of the streaks at $z \approx 50$, we observe a strong growth of the modes e_{11} and e_{13}. This growth is interpreted as a secondary instability of the streaks which leads to a breakdown at $z \approx 300$. Notice that these simulations preserve the symmetry with respect to the attachment line. The anti-symmetric modes $e_{k0}, e_{k2}, \ldots$ (not shown in figure 5) obtain energy through arithmetic noise and grow to a noticeable level only after the breakdown ($z > 300$).

Figure 6 illustrates the effect of the perturbation amplitude for the *slow* perturbation with $f_0 = 1/60$. We find that there is no transition to turbulence for the weakest disturbance ($A_1 = 0.05$, $A_2 = 0.005$). For the two stronger disturbances,

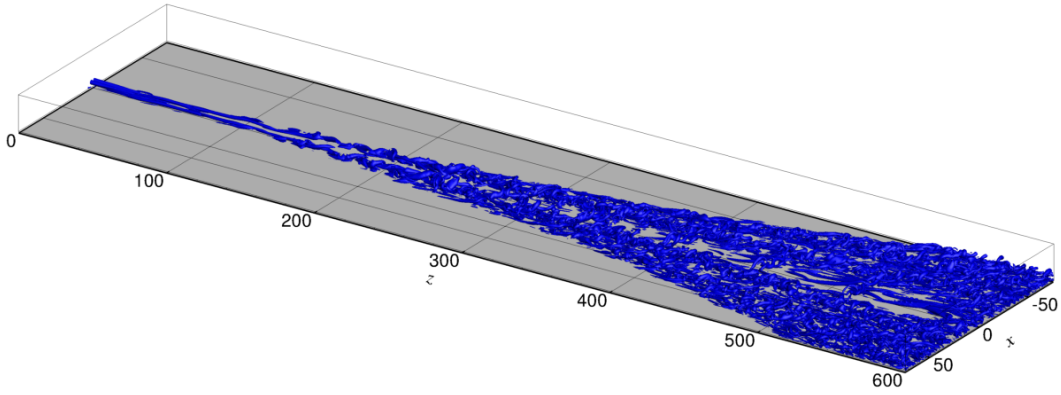

Figure 3. Isosurface of the λ_2 vortex criterion (Jeong & Hussain, 1995) for the *slow III* simulation ($\lambda_2 = -0.001$).

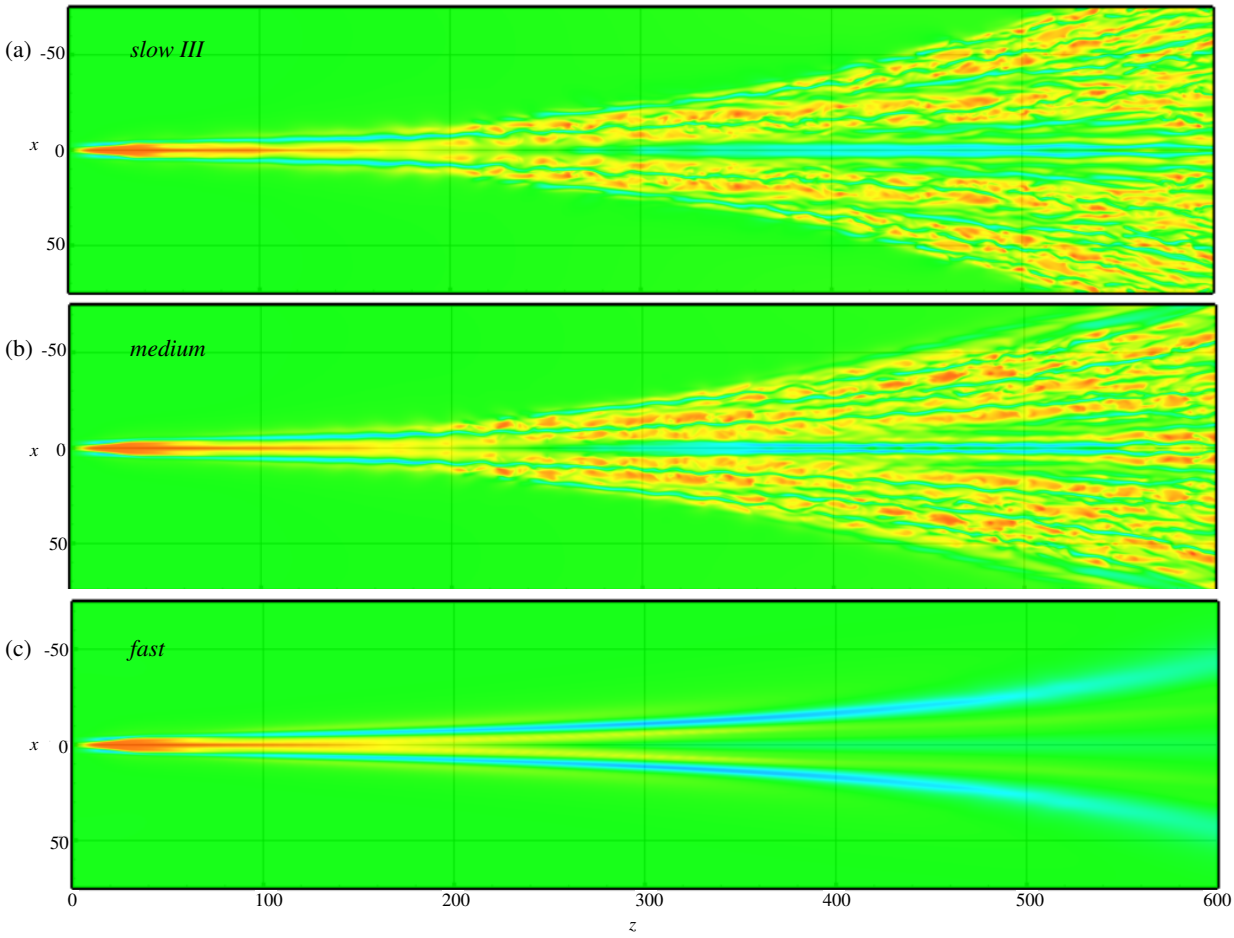

Figure 4. Snapshots of the streamwise velocity in a plane at $y = 1$ (inside the boundary layer). The green color indicates a velocity of $w \approx 0.5$ which corresponds to the base flow configuration, whereas red and blue indicate high and low velocity, respectively.

there is transition and the location of the breakdown to turbulence moves upstream with increasing perturbation amplitude. Case *slow IV* is not shown here. It has a strong primary perturbation amplitude $A_1 = 0.1$ but a weak secondary amplitude, $A_2 = 0.001$. In this case, the secondary instability is not strong enough to bring this case to transition.

So far, we have only investigated secondary perturbations which preserve the symmetry of the base flow. Figure 7 shows the result of a *slow* secondary perturbation which is anti-symmetric. This is achieved by superimposing co-

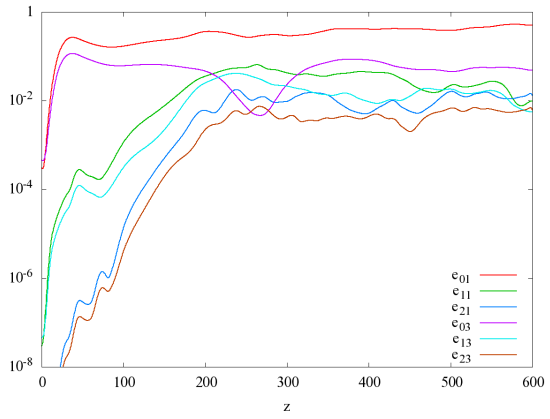

Figure 5. Modal energy densities $e_{kn}(z)$ for the simulation *medium*.

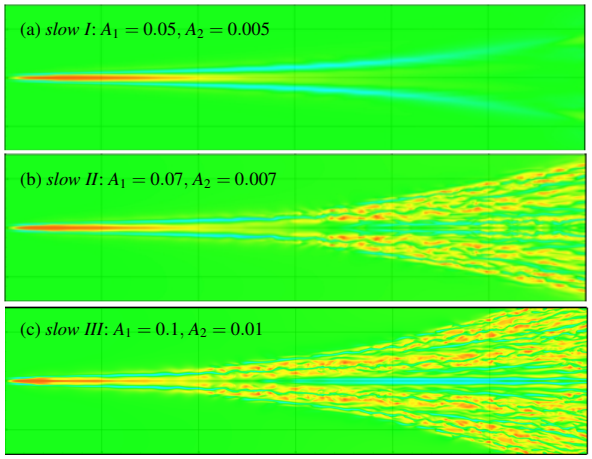

Figure 6. Snapshots of the streamwise velocity in a plane at $y = 1$ (cf. caption and axis labels of figure 4). The three scenarios illustrate the effect of different perturbation amplitudes A_1 and A_2. The frequency of the secondary perturbation is held constant at $f_0 = 1/60$. (Subfigure (c) is identical to figure 4 a.)

rotating vortices onto the counter-rotating vortices of the primary perturbation. The perturbation amplitudes ($A_1 = 0.07$, $A_2 = 0.007$) correspond to the symmetric case shown in figure 6(b).

DISCUSSION

The presented results demonstrate that there are cases for which we obtain subcritical transition to turbulence at $\mathrm{Re} = 300$. Figure 8 summarizes these observations. It is clear that the investigated parameters A_1, A_2 and f_0 are major determinants for the transition process.

It is to be expected that there exists a frequency band within which we can obtain streak breakdown. Our simulations with $A_1 = 0.1$ and $A_2 = 0.001$ suggest that this frequency band lies in a range between $f_0 = 0.01667$ and 0.1. Furthermore, this frequency band appears to widen if we increase the amplitude of the perturbation (cases *slow II & III*). This situation is quite similar to established results for the secondary instability of Tollmien–Schlichting waves as it is illustrated in figure 5 of Herbert (1988).

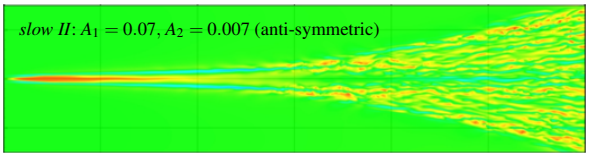

Figure 7. Snapshot of the streamwise velocity in a plane at $y = 1$ (cf. caption and axis labels of figure 4) for an anti-symmetric perturbation with $A_1 = 0.07$, $A_2 = 0.007$ and $f_0 = 1/60$.

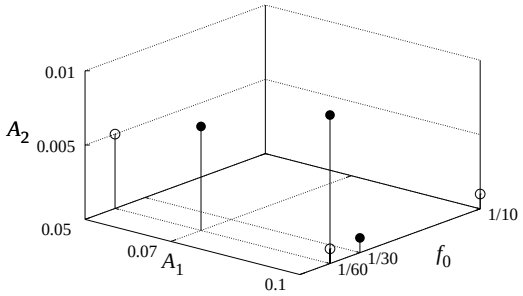

Figure 8. Summary of the studies configurations (cf. table 1): the filled symbols indicate a transition to turbulence, for the open symbols the flow remains laminar.

There exists, however, a subtle difference to the theory for two-dimensional boundary layers: a comparison of cases *slow III* and *slow IV* shows that reducing the secondary amplitude A_2 can *prevent* transition. According to the two-dimensional theory, this would only *delay* the streak breakdown. This phenomenon is probably related to the divergence of the streamwise vortices which effectively limits the region of secondary growth in the downstream direction.

We see that the present problem has a strong three-dimensional character due to the curved streamlines which tend to 'pull the growing perturbations apart' in the chordwise direction. Nevertheless, we can draw some further analogies to the classical theory of secondary instabilities. Figure 9 is adapted from (figure 8.7 in Schmid & Henningson, 2000) for the secondary instability of vortices and streaks in two-dimensional boundary layers. It illustrates the present configuration in the spectral plane. In contrast to the classical version of this diagram, the ordinate indicates the integer polynomial order n in chordwise direction. Therefore, the concept of a *Floquet detuning constant* (Schmid & Henningson, 2000) is limited in this context to integer values. We can distinguish between secondary perturbations which preserve the symmetry of the base flow (filled circles in figure 9) and anti-symmetric perturbations which break the symmetry of the base flow (open circles). In the language of the classical secondary instability theory, the symmetric and anti-symmetric secondary instabilities correspond to fundamental and subharmonic instabilities, respectively.

The simulation for an anti-symmetric secondary perturbation (figure 7) can be directly compared to figure 6(b) which

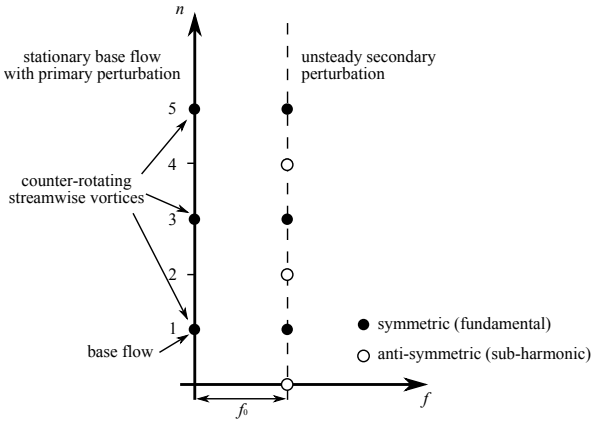

Figure 9. Diagram of the secondary instability in the spectral plane spanned by the chordwise polynomial order n and the frequency f_0.

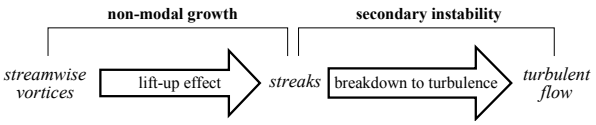

Figure 10. Subcritical transition mechanism observed for swept Hiemenz flow with a pair of counter-rotating streamwise vortices.

is symmetrically perturbed with the same amplitudes. From this particular comparison, it appears that the global picture of the transition process is not influenced by the (anti-)symmetry of the perturbation. One significant difference between the two results can be found between $z = 300$ and $z = 400$ where the symmetric perturbation leads to a varicose instability, while the anti-symmetric perturbation exhibits a sinuous streak instability.

CONCLUDING REMARKS

We presented DNS results for a spatial transition scenario of swept Hiemenz flow at a subcritical Reynolds number of $\mathrm{Re} = 300$. The results suggest that there exists a transition mechanism similar to a bypass transition scenario for two-dimensional boundary layers: (a) streamwise vortices generate streaks in the boundary layer through the lift-up effect; (b) the streaks exhibit a secondary instability whose growth rate depends on the frequency of the secondary perturbation; (c) the laminar vortices break down to turbulence. This transition mechanism is summarized in figure 10.

In order to obtain a more complete picture of the transition process, the study of the parameters A_1, A_2, f_0 must be extended (cf. figure 8). This includes also an investigation of anti-symmetric secondary perturbations. Finally, the configuration of the streamwise vortices at the inflow, e.g. the sense of rotation or the parameters x_c, y_c and b, should be systematically varied to assess its effect on the transition process. Clearly, the transition will be delayed or even suppressed if the streamwise vortices are too far apart.

It is likely that more detailed investigations of the described transition mechanism will allow a reduction of the Reynolds number from $\mathrm{Re} = 300$ toward the critical Reynolds number observed experimentally by Poll (1979).

REFERENCES

Dimas, A. A., Mowli, B. M. & Piomelli, U. 2003 Large-eddy simulation of subcritical transition in an attachment-line boundary layer. *Computers & Mathematics with Applications* **46** (4), 571 – 589.

Guégan, A., Schmid, P. J. & Huerre, P. 2008 Spatial optimal disturbances in swept attachment-line boundary layers. *J. Fluid Mech.* **603**, 179–188.

Hall, P., Malik, M. R. & Poll, D. I. A. 1984 On the stability of an infinite swept attachment line boundary layer. *Proc. R. Soc. Lond.* **A 395**, 229–245.

Hall, P. & Malik, M. R. 1986 On the instability of a three-dimensional attachment-line boundary layer: Weakly nonlinear theory and a numerical approach. *J. Fluid Mech.* **163**, 257–282.

Henniger, R., Kleiser, L. & Meiburg, E. 2010*a* Direct numerical simulations of particle transport in a model estuary. *J. Turbulence* **11** (N 39), 1468–5248.

Henniger, R., Obrist, D. & Kleiser, L. 2010*b* High-order accurate solution of the Navier–Stokes equations on massively parallel computers. *J. Comp. Phys.* **299** (10), 3543–3572.

Herbert, T. 1988 Secondary instability of boundary layers. *Annu. Rev. Fluid Mech.* **20**, 487–526.

Jeong, J. & Hussain, F. 1995 On the identification of a vortex. *J. Fluid Mech.* **285**, 69–94.

Joslin, R. D. 1995 Direct simulation of evolution and control of three-dimensional instabilities in attachment-line boundary layers. *J. Fluid Mech.* **291**, 369–392.

Landahl, M. T. 1980 A note on an algebraic instability of inviscid paralel shear flows. *J. Fluid Mech.* **98**, 243–251.

Lin, R.-S. & Malik, M. R. 1996 On the stability of attachment-line boundary layers. Part 1. The incompressible swept Hiemenz flow. *J. Fluid Mech.* **311**, 239–255.

Obrist, D. & Schmid, P. J. 2003*a* On the linear stability of swept attachment-line boundary layer flow. Part 1. Spectrum and asymptotic behaviour. *J. Fluid Mech.* **493**, 1–29.

Obrist, D. & Schmid, P. J. 2003*b* On the linear stability of swept attachment-line boundary layer flow. Part 2. Non-modal effects and receptivity. *J. Fluid Mech.* **493**, 31–58.

Poll, D.I.A. 1979 Transition in the infinite swept attachment line boundary layer. *Aero. Q.* **30**, 607–629.

Schmid, P. J. & Henningson, D. S. 2000 *Stability and Transition in Shear Flows*. Springer.

Spalart, P. R. 1988 Direct numerical study of leading-edge contamination. In *Proceedings of the AGARD Symposium on Application of Direct and Large Eddy Simulation to Transition and Turbulence*, *AGARD* CP-438, pp. 5-1–13.

Theofilis, V. 1995 Spatial stability of incompressible attachment-line flow. *Theoret. Comput. Fluid Dynamics* **7**, 159–171.

Theofilis, V., Fedorov, A., Obrist, D. & Dallmann, U. C. 2003 The extended Görtler-Hämmerlin model for linear instability of three-dimensional incompressible swept attachment-line boundary layer flow. *J. Fluid Mech.* **487**, 271–313.